Precision Engineering 52 (2018) 440–450

Contents lists available at ScienceDirect

Precision Engineering

journal homepage: www.elsevier.com/locate/precision

Nanosecond pulsed laser irradiation of sapphire for developing microstructures with deep V-shaped grooves

Nozomi Takayama[a], Shouhei Asaka[b], Jiwang Yan[a,*]

[a] Department of Mechanical Engineering, Keio University, Hiyoshi 3-14-1 Kohoku, Yokohama, Kanagawa 223-8522, Japan
[b] Shinkosha Co., Ltd., 2-4-1 Kosugaya Sakaeku, Yokohama, Kanagawa 247-0007, Japan

ARTICLE INFO

Keywords:
Laser processing
Optical element micromachining
Sapphire
Groove formation
Taper formation
Microstructure
Hard brittle material

ABSTRACT

A nanosecond pulsed Nd:YAG laser was used to irradiate a sapphire substrate to produce 3-dimensional microstructures with sharp V-shaped grooves. In initial experiments, where single grooves were machined, a maximum taper angle of ~79° was obtained. At constant laser parameters, the taper angle remained constant. As the taper angle increases from a flat surface, the irradiated area increases while incident fluence decreases; once the incident fluence approaches the ablation threshold, the taper angle becomes constant. The taper angle could be controlled by the laser fluence, scanning speed and incident angle of the laser beam. Using these results, a kind of surface microstructure, comprised of micropyramids with steep walls, was successfully machined for optical measurement applications. The surface roughness, transmittance and crystallinity of the microstructure surface could be controlled by the laser scanning speed. By applying the taper formation mechanism proposed in this study, the micromachining of sharp microstructures with steep walls on various hard brittle materials becomes possible.

1. Introduction

Sapphire is a useful material in a wide range of applications, due to its high hardness, strength, wide band-width transparency and chemical inertness. In recent years, sapphire is increasingly used in many optical devices, optic fibers and LED substrates [1–3]. Due to its superior properties such as greater resistance to scratches and abrasion, it is expected to replace glass materials as a display screen material. Moreover, to meet the growing demand for sapphire as LED substrates, technologies for the crystal growth and surface processing of synthetic sapphire have been extensively developed, resulting in the reduction of production costs. This has also stimulated the use of sapphire in new applications. Despite having great potential as a highly functional material, sapphire is very difficult to machine due to its high hardness and brittleness [4]. It is difficult to process microstructures such as holes and grooves, with sub-millimeter feature sizes by conventional mechanical means. For example, if the ultrasonic drilling of sapphire is attempted, there is a possibility of tool breakage by chips filling the drill hole [5]. In addition, mechanical machining of sapphire causes high levels of tool wear, making it incredibly difficult to achieve high shape repeatability.

Therefore, many researchers have turned to non-conventional methods in order to machine sapphire microstructures at a high level of precision. To avoid the problems of tool breakage and wear present in mechanical methods, the primary focus has been on non-contact methods. The etching of sapphire is often performed to process wafer substrates but it is known to be time-consuming and requires a masking process. Sapphire is commonly etched by a $3H_2SO_4$:$1H_3PO_4$ mixture solution at 300–400 °C. Some studies have reported that it takes 10 h to machine a square area of 0.5 × 0.5 mm to a depth of 0.09 mm [6,7]. Therefore, etching is unsuitable for the machining of deep structures.

Laser machining can be applied as a more rapid method, with the additional advantage of high geometrical freedom. It is easy to create complex shapes by controlling and scanning the laser beam. Ultra-short pulsed laser machining has been successfully applied for the ablation of sapphire [8]. However, it must be taken into account that not only is the equipment for this method very expensive, the material removal rate is low. Thus it is unsuitable for the machining of large areas. In order to achieve a higher material removal rate at a lower cost, the use of a nanosecond pulse may be more suitable. Previous studies have shown that a nanosecond pulse can be used to machine small holes into sapphire with high precision [2]. A longer pulse, such as one of a microsecond order, however, would result in a large heat affected zone. As sapphire is both brittle and a poor thermal conductor, many cracks may form after long-pulse laser irradiation.

The laser machining of sapphire is not without its problems. One of

* Corresponding author.
E-mail address: yan@mech.keio.ac.jp (J. Yan).

https://doi.org/10.1016/j.precisioneng.2018.02.008
Received 3 February 2018; Accepted 12 February 2018
Available online 16 February 2018
0141-6359/ © 2018 Elsevier Inc. All rights reserved.

Downloaded from Yan Laboratory, Keio University at http://www.yan.mech.keio.ac.jp. Redistribution is subject to copyright licence from the journal publisher.

the greatest and least understood problems is the formation of a taper, especially when machining deep structures. A taper results when the entrance diameter or groove width is greater than the exit diameter or width. This is a pressing problem as many applications of sapphire require a high aspect ratio without a taper or, conversely with a specific taper angle. Taper formation due to laser machining is not uncommon; it is thought to occur primarily due to inherent focusing properties of the laser; laser power is reduced by beam propagation [9–11]. Thus it was found that focal plane position has a significant effect on taper formation. Some researchers have found that other parameters, specifically laser fluence and pulse number, also affect the taper angle [12]. However, much of the preceding research is focused on the laser machining of metal materials. Sapphire, as a transparent and brittle material, is expected to have a different response. Additionally, it is agreed that the taper formation is difficult to understand due to complex and interacting phenomena; melting/vaporization, plasma formation, heat and mass transfer. Therefore, it is necessary not only to identify the contributing factors of taper formation but to understand how the taper develops and to apply this understanding to control the taper angle.

Much research has been devoted to removing the laser-induced taper [13–15]. However, this study aims to apply it to three-dimensional machining. By understanding the mechanism behind taper formation, it becomes possible to machine three-dimensional structures with feature sizes of sub-millimeter order. For example, a pyramidal structure can be machined by combining tapered grooves. Such structures have resulted in a low reflectivity in the millimeter wave band [16]. Moreover, due to the sloped walls, the structure's surface retains this low reflectivity over a wide band width [17]. This property is essential for optical elements involved in the measurement of cosmic microwave background radiation (CMB). By applying the taper formation mechanism in laser micromachining, it becomes possible to machine sharp structures. Such structures have not been achieved in previous studies, even with the use of a femtosecond pulsed laser, which is generally used to create highly defined structures.

Thus, in this study, we will investigate the development of the taper angle of deep grooves in sapphire. Various laser parameters will be considered to understand their respective influences on taper development. The results and findings obtained from this study will be extended to developing an efficient method for the machining of typical three-dimensional structures, namely a pyramidal structure for optical elements used in CMB measurement. The understanding of the taper formation phenomena is expected to contribute not only to the laser drilling and cutting of sapphire, but also to the laser machining of other brittle and transparent materials, such as diamond and glass.

2. Experimental method

The laser used in the following experiments was LR-SHG, a Nd:YAG laser pumped by a laser diode, from MegaOpto Co., Ltd. It has a maximum power output of 1W, a wavelength of 532 nm and a spot diameter of 85 μm. The laser output energy has a Gaussian distribution. The laser beam scanning was controlled in two dimensions using a galvanometer scanner system. The laser beam was focused onto a stage using an fθ lens. The sapphire used is a single-crystal cube with a length of 10 mm, produced by Shinkosha Company. It was annealed to remove all internal residual stress and to prevent this from affecting the irradiation results. The plane parallel to the optical axis of the crystal (c-axis) was irradiated. The sample surface was prepared by grinding and the surface roughness of the irradiated plane was 1.02 μmRa.

A specific laser irradiation scheme was used, as presented in Fig. 1. Fig. 1a shows the scheme for groove machining. A single line was irradiated, then the laser beam was moved a pitch of 42.5 μm (half of the beam diameter) across and a second line irradiated. 7 lines was irradiated to form a single groove. Fig. 1b shows the scheme for pyramid irradiation. A thick line represents a single groove as machined by the scheme of Fig. 1a. The vertical grooves are irradiated first, then followed by the horizontal grooves. The combination of the irradiation of the 2 groove sets are counted as 2 irradiation times. In this way, a 3 × 3 pyramidal structure was machined. The parameters used are shown in Table 1.

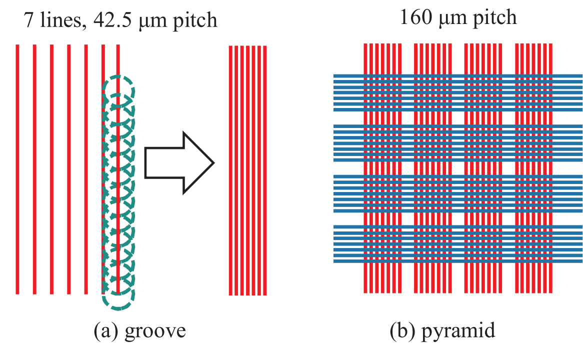

Fig. 1. The laser irradiation scheme used for the machining of (a) a groove and (b) a pyramid structure.

Table 1
Experimental laser parameters.

Laser parameters	Value
Wavelength (nm)	532
Pulse width (ns)	15.4
Repetition frequency (kHz)	1
Fluence (J/cm^2)	7.4, 10.6, 12.5, 15.7
Scanning speed (mm/s)	0.5, 5
Irradiation times	1, 5, 10, 15 (for 0.5 mm/s) 1, 10, 50, 150 (for 5 mm/s)

After irradiation, the samples were observed using the Inspect S50 Scanning Electron Microscope (SEM) made by FEI Company for confirming the surface structure. A MP-3 laser probe profilometer made by Mitaka Kohki Co., Ltd. was used to measure groove profile and depth. A laser microscope VK-9700 made by Keyence Corporation was used to measure the surface roughness. In addition, sound generation during machining was measured and analyzed by a High Function Sound Level Meter LA-3560 made by Ono Sokki Co., Ltd.

3. Simulations of temperature

A simulation was performed to investigate the temperature after irradiation by a pulsed laser. COMSOL Multiphysics software was used in the following simulations. A geometry, similar to that of the actual sapphire samples used in the experiments, was employed, where the z-axis was directed into the material, with the origin at the surface. The maximum temperature of the sapphire during laser irradiation was calculated. Heat transfer during a nanosecond pulsed irradiation occurs through thermal conduction; a conduction model was applied using the following equations.

$$\mathrm{d_z}\rho \mathrm{c_p}\left(\frac{\partial \mathrm{T}}{\partial \mathrm{t}}\right) + \nabla\cdot \mathrm{q} = \mathrm{q_0} \tag{1}$$

$$q = -\mathrm{d_z} k \nabla T \tag{2}$$

where T is the temperature, q is the heat intensity, ρ is the density, c_p is the specific heat capacity and k is the thermal conductivity of the material. As the laser spot size and the heated region are small compared to the thickness of the sapphire sample, the temperature of the bottom surface of the sample is thought to be maintained at ambient temperature. The heat input Q_{in} to the material delivered by a single pulse of the laser is given by

$$\mathrm{Q_{in}}(r, t) = A{*}I_0(t){*}\alpha{*}\exp(-\alpha z){*}\exp\left(\frac{-2r^2}{R^2}\right){*}\mathrm{f}_{\mathrm{tri}(t)} \tag{3}$$

Table 2
Properties of sapphire used in simulation.

Properties	Value
Absorption coefficient (cm^{-1})	4771.4
Absorptivity	0.15
Emissivity	0.48
Density (kg/m^3)	3987
Specific heat capacity (kJ/K kg)	0.75
Thermal conductivity (W/m K)	42

where A is the absorptivity of the material, $I_0(t)$ is the laser pulse energy, α is the absorption coefficient, r is the distance from the beam center and R is the beam radius. The function exp(-αz) represents the optical penetration depth of the laser beam into the material. The functions, exp(-2r^2/R^2) and $f_{tri}(t)$, model the Gaussian distribution of the beam energy and the triangular pulse function respectively. This heat input was applied to the surface. Radiation from the irradiated surface was modelled by the equation below.

$$-\ \mathrm{n}\cdot q = \mathrm{d}_z \varepsilon\sigma (T_{\mathrm{amb}}^4 - T^4) \quad (4)$$

where ε is the surface emissivity and T_{amb} is the background temperature of 293 K. A wavelength of 532 nm, pulse width of 15.4 ns, beam radius of 42.5 μm, power of 0.89 mW was applied to the model. The properties of sapphire used in the simulation are shown in Table 2.

4. Results and discussion

4.1. Effect of consecutive irradiations

As it is imperative that the initial taper formation is understood, stationary pulse irradiation, which is less complex compared to groove irradiation, will first be investigated. 1 pulse leaves no mark; at least 10 pulses are needed to create a clear irradiation mark as shown in Fig. 2a. This is thought to be due to the low initial absorptivity of sapphire in its solid state. Once it is molten, its absorptivity rises dramatically and a melt pool forms [18]. A mark machined by 50 stationary pulses has a taper as in Fig. 2b. This is thought to be due to the beam's Gaussian distribution inducing a temperature distribution, and consequently, a melt layer depth distribution. This distribution agrees well with the simulation result, presented in Fig. 3. This shows that the region exceeding the melting temperature of sapphire corresponds to a smooth curve.

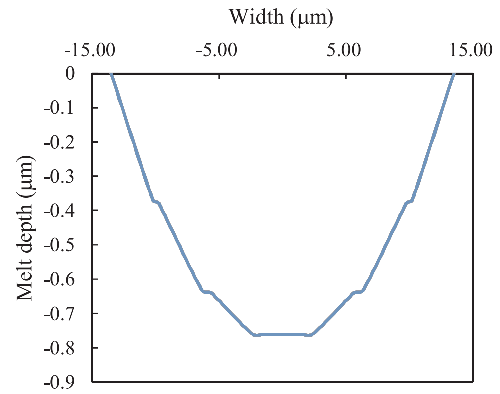

Fig. 3. SEM images showing the cross-section of the groove after: (a) 1, (b) 5, (c) 10, (d) 15 irradiation times.

From the calculated result, the initial temperature distribution is not sharp. From the experimental results, there is no V-shape as observed in the drilled holes at pulse numbers of 50 and below. However, when an increasing number of pulses are irradiated, up to 80 pulses, the center of the irradiation point is preferentially machined, as in Fig. 2c. This results in a sharper V-shape and a small hole at the center, as indicated

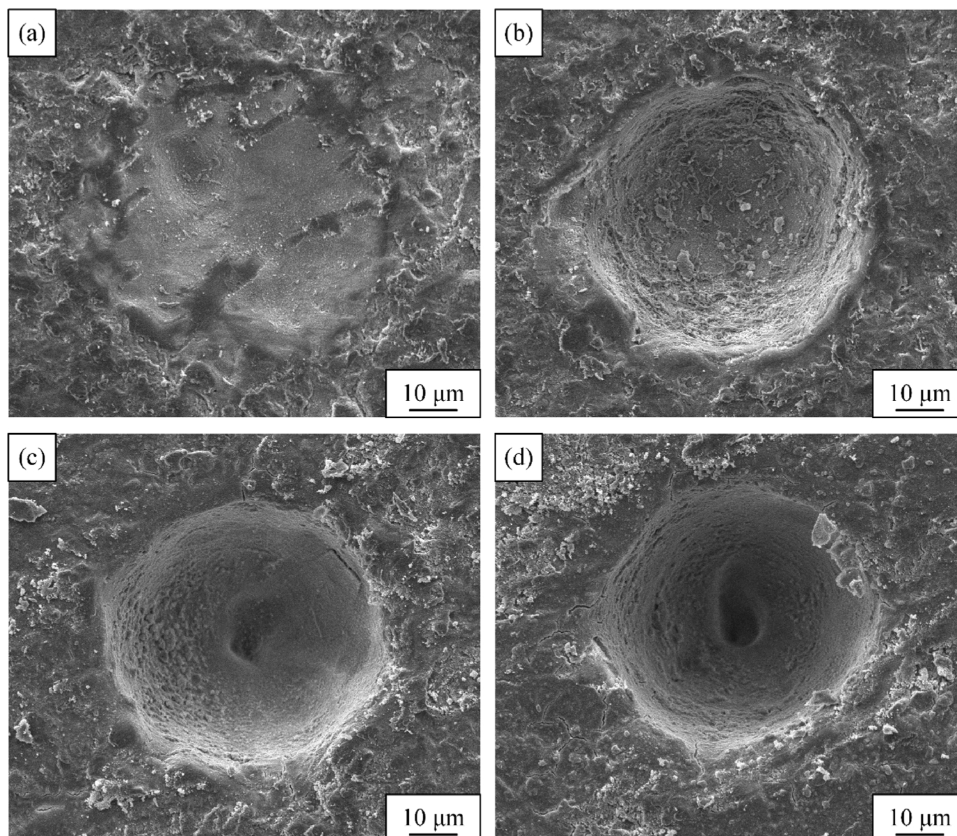

Fig. 2. The cross-sectional profiles of grooves machined with a varying number of times.

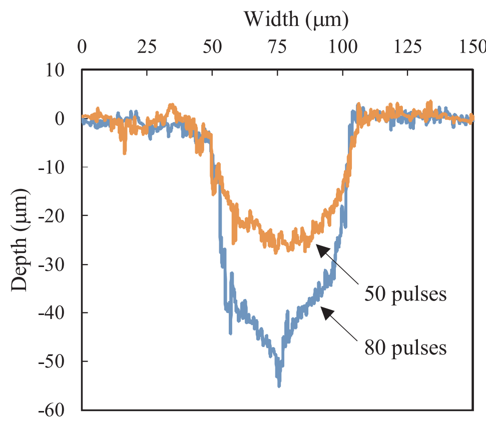

Fig. 4. A model of the developing groove; (a) with an increasing taper angle and (b) a constant taper angle.

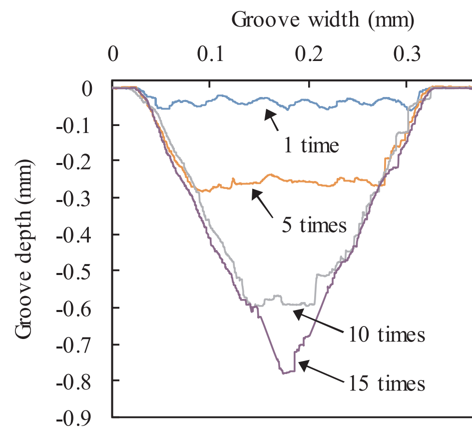

Fig. 5. SEM images of stationary point irradiation with: (a) 10, (b) 50, (c) 80, (d) 100 pulses.

by the cross-sectional profile of Fig. 4. It is interesting to note that the regions near the edge of the hole are not machined further between 50–80 pulses. This is thought to be due to a plasma shielding effect. At ambient pressure, the laser-induced plasma is known to become more confined; it does not expand rapidly into the surrounding area [19,20]. The expansion front is slowed by coalesces with slower components in the ambient atmosphere; thus the plume remains very close to the target surface. The effective length of the plasma is reduced and the lifetime is known to be much longer. Thus a high density and long-lasting plasma accumulates in the irradiated region and shields the region from subsequent pulses. If the plasma is dense enough, it may prevent further machining.

Considering the plasma, in order for laser pulses to reach and machine the hole bottom, an increased intensity is needed. At larger hole depths, the hole walls are steep enough to reflect incoming laser light to the center of the machined hole. This reflected light is directed towards the center of the hole so that an increased intensity is irradiated in this region. If this combination of incoming laser intensity (some of which is shielded by the plasma) and the reflected intensity is greater than the machining threshold of sapphire, the center of the hole can be machined. This causes the deepening of only a limited central area and finally results in the particular shape observed after irradiation with over 50 pulses.

Another possible explanation for the peculiar hole shape is temperature dependency of energy absorption. At the center of the hole, the temperature is higher and the absorption coefficient, which possesses temperature dependency, may be higher. Therefore, a greater amount of energy is absorbed leading to greater material removal from the center. However, this implies that the difference in material removal from the edge and from the center is dependent on the temperature distribution or the beam's energy distribution. As this is constant throughout the machining process, it cannot explain the sudden appearance of the small center hole.

The above discussion implies that machining occurs via 2 different regimes. First, the machining proceeds by melting and ejection of the melted material. The Gaussian laser energy distribution causes the formation of a temperature distribution in the irradiated spot and causes the hole to narrow. As the area of the hole bottom becomes smaller, the ejected material has less space to expand, leading to the accumulation of a high density plasma at the bottom of the hole. At the critical point of 80 pulses, the plasma is dense enough to prevent machining near the edge of the hole. However, at the center, the addition of reflected intensity allows the total incident intensity to exceed the machining threshold of sapphire, and deepening of the hole center occurs. Thus it is possible for a sharp shape to be machined even with a Gaussian distribution. This sharp shape is considered to the starting point of a tapered wall.

Next, the groove development phenomenon was investigated by irradiating grooves with various irradiation times at a laser fluence of 15.7 J/cm^2, a scanning speed of 0.5 mm/s. The cross-sectional profiles of the grooves after a varying number of passes are shown in Fig. 5. The SEM images of the corresponding grooves are shown in Fig. 6. Both figures indicate that a deep, tapered groove was machined. The maximum groove depth is much smaller than the laser Rayleigh length of 10 mm, thus variations of the beam radius can be ignored. As can be seen from Fig. 6a, the 1st irradiation time results in a sloped wall. As machining proceeds, the groove shape changes from a trapezoid to a V groove. The tapered groove reaches a certain maximum depth when the 2 tapered walls of the groove meet.

The cross-sectional profiles show that, from 5 times and above, the groove propagates into the bulk material at a constant taper angle. The fact that the taper angle does not change with consecutive passes indicates that the groove is not machined from a profile with a gradual curve to a steeper curve as shown in Fig. 7a. Rather, it is machined as presented in Fig. 7b, where the angle is decided at a low number of passes and the taper angle is constant throughout machining. Thus, it would be possible to estimate the maximum attainable depth from a low number of passes.

In order to distinguish between various structures, the V shaped groove will be referred to as a groove while the smaller grooves resulting from a single line irradiation will be referred to as marks. Focusing on the back wall of the groove, in the region near the entrance side of the groove (near the original surface), gradual narrowing of the marks can be observed in the vertical direction, as indicated by Figs. 8a and b. As the mark progresses into the material, the mark becomes thin, almost crack-like, as in Fig. 8c. This is a similar phenomenon to the stationary pulse irradiation which showed a sudden narrowing of the hole. Referring to the previous discussion, the initial narrowing increases the plasma density within the mark, and only the center area, which receives intensity reflected from the walls, can be machined. As the mark grows narrower, the ridges on either side become more layered and this is thought to be due to material accumulation. This further supports the discussion that material melted by laser heating cannot be completely ejected from the mark as it accumulates on the ridges [21]. A smaller amount is completely ejected from the sample surface at deeper regions, resulting in layered ridges in these regions. This further contributes to the narrowing of the machined area.

The amount of the ejected material was also estimated by measuring the sound emitted during consecutive passes; the resulting power spectrum is shown in Fig. 9. The sound is known to correspond with the amount of particles emitted from the surface into the surrounding atmosphere [22]. The sound from the 1st time and the 5th time are compared. When the groove is deeper, a smaller noise is emitted. Thus it can be concluded that the melted particles are hardly ejected from

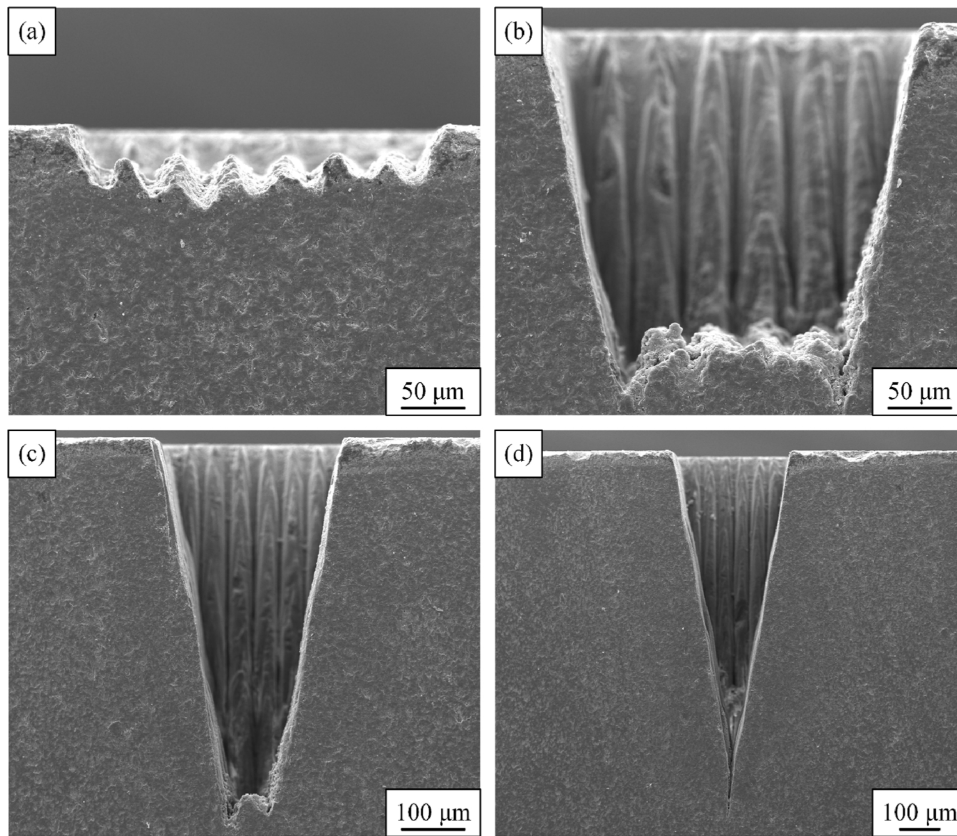

Fig. 6. Simulation result showing the contour of T = 2313 K (the melting point of sapphire).

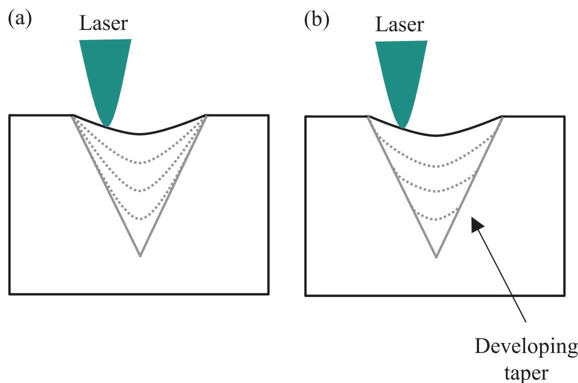

Fig. 7. The cross-sectional profiles of the holes formed by stationary point irradiation.

deeper regions and instead accumulate on the walls of the machined area.

Additionally, in these regions, stripe-like periodic structures can be observed, as seen in Fig. 8d. The distance between neighboring stripes is < 2 µm, which is similar to the wavelength of the laser used, so it is likely to be due to interference between reflected laser light [23,24]. The vertical walls of the mark are not parallel to the laser beam propagation direction; this facilitates and increases the possibility of multiple reflections and interference. In addition, if the mark is too wide, light may be absorbed by the plasma and decrease in intensity while it is transmitted.

Next, the groove bottom of 1 and 5 irradiation times, shown in Fig. 10, will be compared. After 1 time, the individual marks are distinguishable as shown in Fig. 10a. The distinct marks are due to limited machining occurring in the outer regions of the laser beam, as these regions have lower intensities. However, with 5 times, the marks are not distinct as shown in Fig. 10b. This change in surface structure is thought to be due to the surface roughness increasing and the damage threshold decreasing after 1 irradiation time. After 1 irradiation time, the surface roughness increases from 1.02 to 3.61 µmRa. An increased surface roughness causes electric field enhancement, which in turn leads to a smaller damage threshold and greater material removal, when the pulse width is above 0.15 ns [25]. Thus, it can be assumed that in the following irradiation times, increased material removal occurs even in the regions of the beam with low laser fluences. This results in the machining of the wall in between neighboring irradiation passes and the individual marks become less distinct.

In addition, many circular droplets of debris can be observed on the surface after 5 irradiations, covering the irradiation marks, as in Fig. 10b. Circular droplets are believed to be formed by the outflow of melted material from pits to humps in multi-pulse relief formation [26]. When melted material flows around pits, it experiences centrifugal force, inducing a Rayleigh-Taylor instability at the liquid-vapor interface, causing the droplet to be ejected from the surface. In the case of 5 irradiation times, as the groove is deeper, the debris cannot be completely ejected from the surface, leading to increased redeposition and accumulation on the groove bottom.

4.2. Effect of focal plane position

The influence of the focal plane position must also be considered here. Previous studies involving the taper drilling of metals found that focal plane position greatly affected the taper angle [27]. In order to investigate, a line was machined where the focal plane position was set to 0 µm, −85 µm respectively after each irradiation time and the groove depth was measured. In the machining of a V groove, the taper angle is decided by the gradient of the groove walls when the V shape is fully formed. This gradient is equivalent to the depth of the groove divided by the width of the groove. Therefore, the groove depth corresponds to the taper angle. As a single pass at a scanning speed of

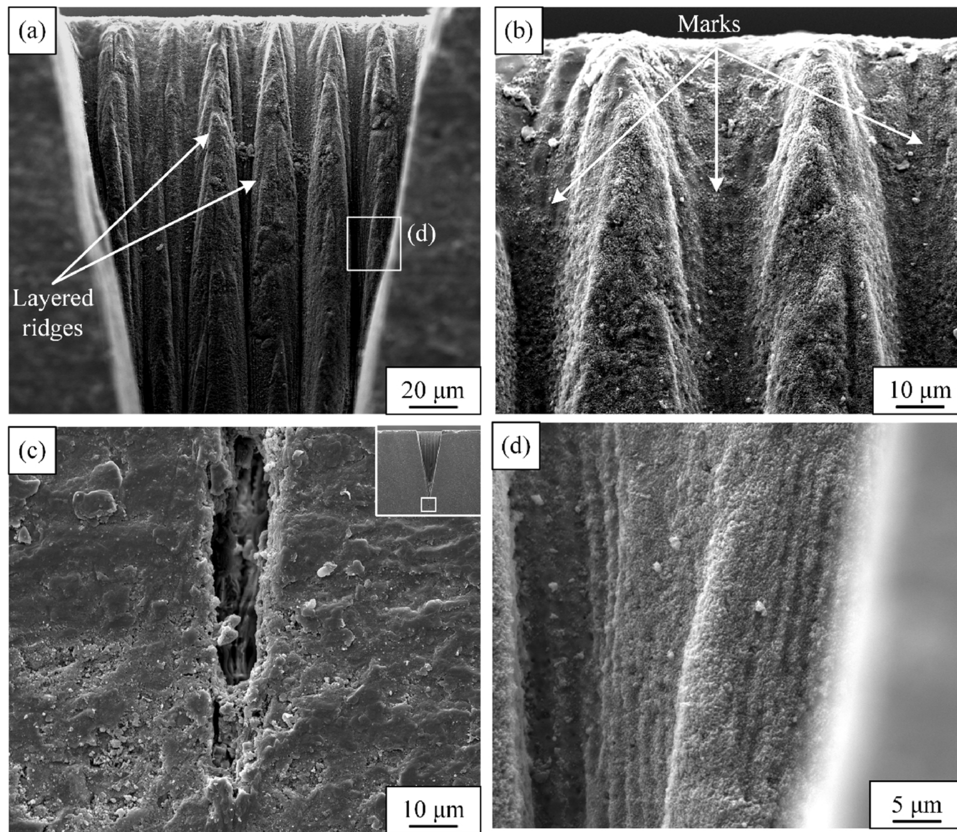

Fig. 8. SEM images of a groove machined by a fluence of 15.7 J/cm^2, a scanning speed of 0.5 mm/s and 15 irradiation times showing (a) the back wall of the groove; (b) the vertical narrowing of the marks; (c) the bottom of the groove with the entire groove inset; (d) interference fringes.

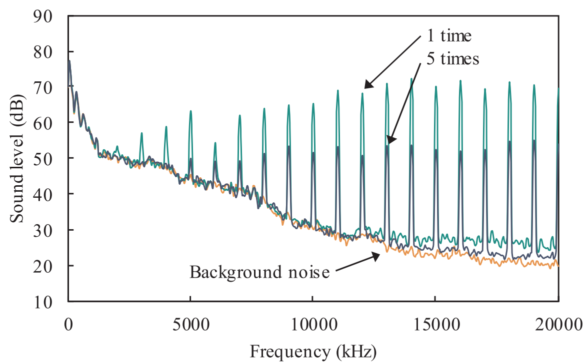

Fig. 9. The power spectrum of the sound emitted during the machining of sapphire.

1 mm/s has a depth of 30 µm, no displacement results in a positive plane position and one of −85 µm results in a negative plane position. The depths of the groove are presented in Fig. 11. By comparing the depths, no significant difference can be found. In this experimental range, focal plane position is thought to have little effect on the machining process. This is thought to be due to the laser system used. The laser beam has a large Rayleigh length of roughly 10 mm. This results in the beam radius varying only a slight amount and having a value of 42.7 µm at a depth of 1 mm. Therefore, the laser beam can be considered as almost cylindrical throughout the depth of the groove. Thus the groove is unaffected by small variations in focal plane position. It may begin to exert a larger influence when a much larger depth is machined.

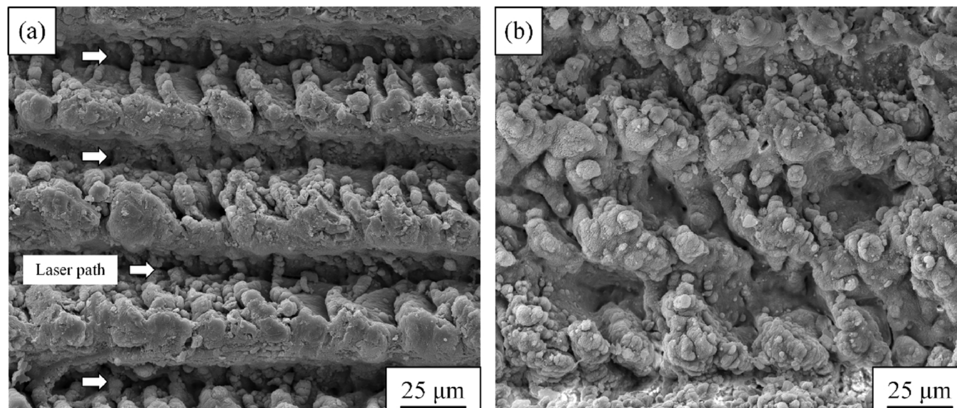

Fig. 10. SEM images of the groove bottom after (a) 1, (b) 5 irradiation times.

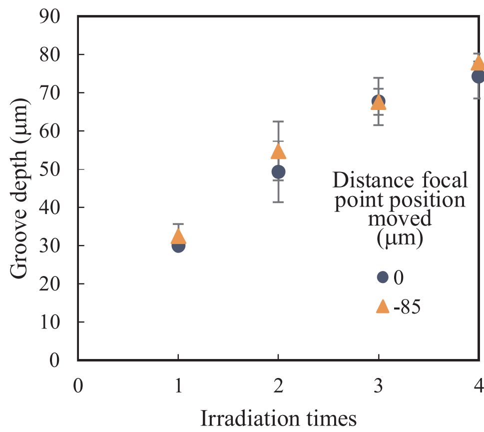

Fig. 11. Groove depth in relation to the irradiation times at different focal point positions.

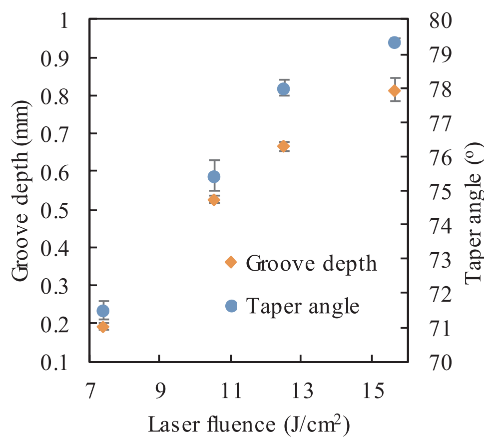

Fig. 12. Groove depth and taper angle in relation to the laser fluence.

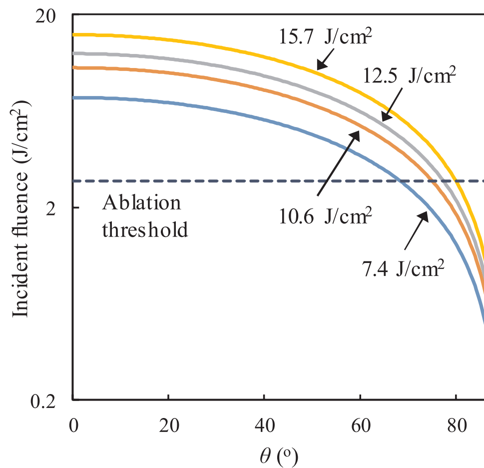

Fig. 13. The incident laser fluence in relation to the taper angle.

Table 3
Comparison of calculated and experimentally obtained values for the maximum taper angle.

Laser fluence (J/cm^2)	Calculated angle (°)	Experimentally obtained angle (°)
7.4	68.0	71.5 ± 0.3
10.6	75.1	75.4 ± 0.4
12.5	77.4	78.0 ± 0.2
15.7	80.0	79.4 ± 0.1

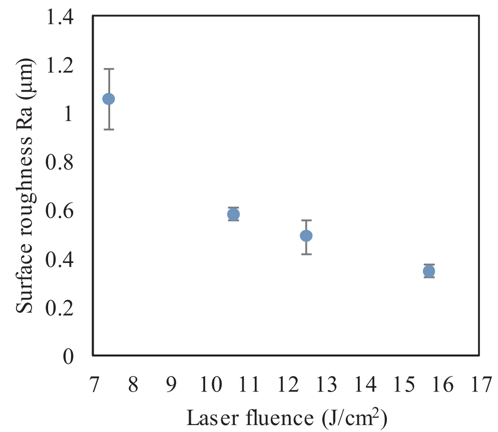

Fig. 14. Surface roughness of the groove walls in relation to the laser fluence.

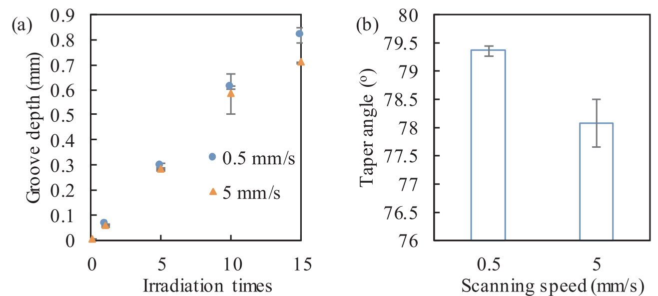

Fig. 15. (a) Groove depth in relation to irradiation times and (b) taper angle at different scanning speeds.

4.3. Effect of laser fluence

Machining of grooves was carried out at a constant scanning speed of 0.5 mm/s and 15 times. The depths and taper angles of the grooves machined by various laser fluences are shown in Fig. 12.

From Fig. 12, there appears to be a relationship between the taper angle and the laser fluence. This is due to the machining threshold. Consider the area of the laser beam incident on the tapered walls of the groove when the wall taper angle is θ. Assuming a sufficiently large Rayleigh length, the beam area incident on the groove wall A_{taper} is larger than the beam area incident on a flat surface A. This assumption is valid as the effect of the focal plane position was shown to be negligible in the previous section. The areas can be written by the following equation.

$$A_{taper} = \frac{A}{\cos\theta}$$

Next, the laser fluence at the two areas will be considered. The laser power P is constant throughout the beam. Therefore, the following relation is obtained.

$$F_{taper} = \frac{P}{A_{taper}}$$

As θ increases, the incident fluence F_{taper} decreases as shown in Fig. 13. In order for material removal to occur, the incident fluence must be greater than the machining threshold of sapphire.

The machining threshold, the minimum power required for machining to occur, can be empirically determined by measuring the diameter of the hole created by laser pulses, as shown in Fig. 5 As indicated by Fig. 5, the machining threshold is obtained at r = 30 µm, where r is the distance from the center of the irradiation spot. The threshold power is 155 mW. Therefore, the machining threshold fluence at 0° is 2.73 J/cm^2.

Table 3 shows the calculated and experimentally obtained

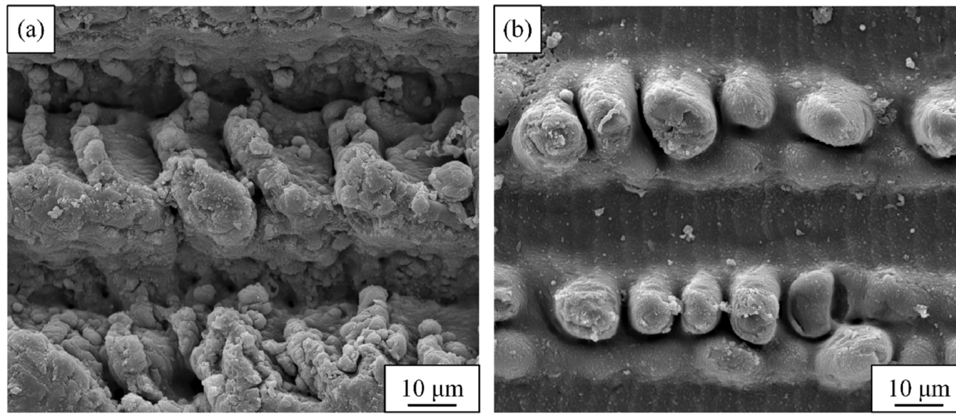

Fig. 16. SEM images of the groove bottom machined at laser scanning speeds: (a) 0.5 mm/s, (b) 5 mm/s.

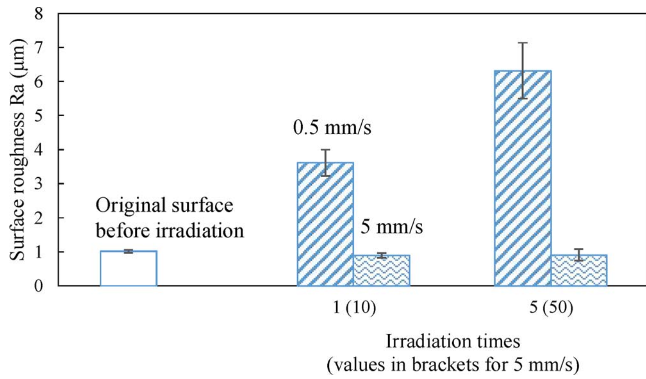

Fig. 17. Surface roughness of irradiated sapphire sample.

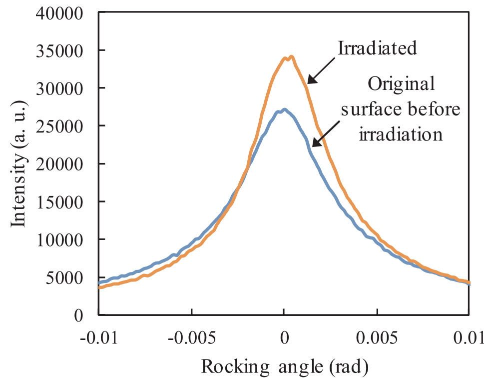

Fig. 18. X-ray rocking curve of the sapphire sample before and after irradiation.

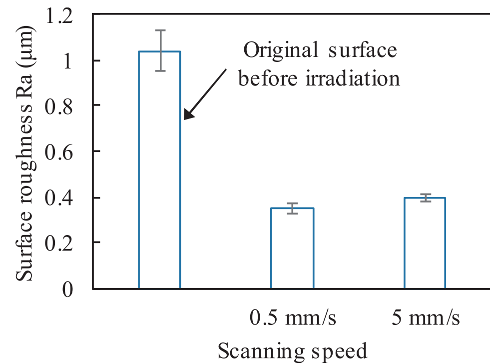

Fig. 20. Surface roughness of the groove wall.

maximum taper angles. For high fluences, a good agreement is observed. However, a large discrepancy can be observed between the calculated and measured values at a low fluence. As the experimentally obtained angle is larger than the theoretical value, it implies that more laser energy is absorbed than theoretically. This may be due to incomplete machining resulting in larger surface roughness along the groove walls at a low fluence, as indicated by Fig. 14. This may lead to increased material removal and a greater taper angle.

4.4. Effect of scanning speed

Machining of grooves was carried out at a constant fluence of 15.7 J/cm^2 and 15 times at different scanning speeds. The groove depths and the resulting taper angles are shown in Fig. 15. From Fig. 15a, the groove depths are initially the same. But a higher scanning

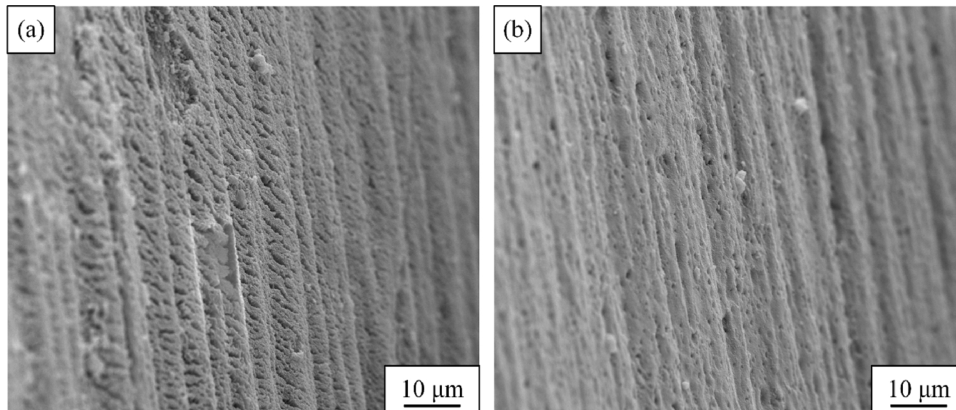

Fig. 19. SEM images of the groove wall machined at laser scanning speeds: (a) 0.5 mm/s, (b) 5 mm/s.

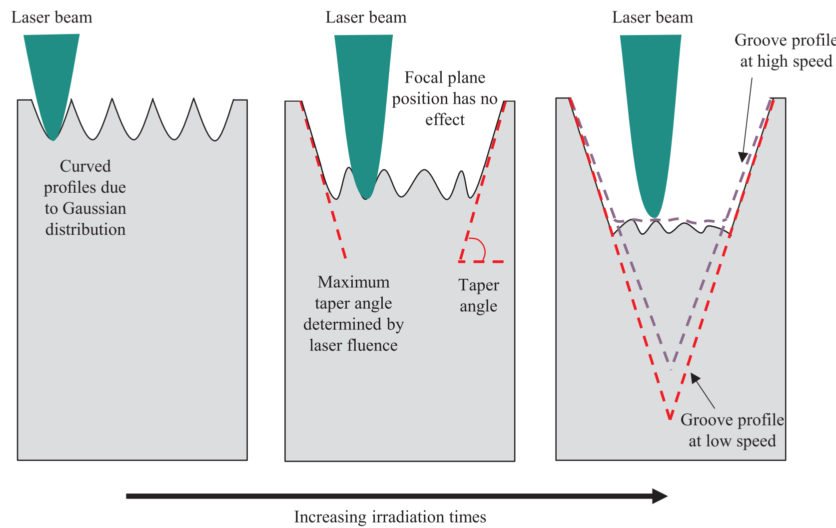

Fig. 21. Mechanism of taper formation with increasing irradiation times.

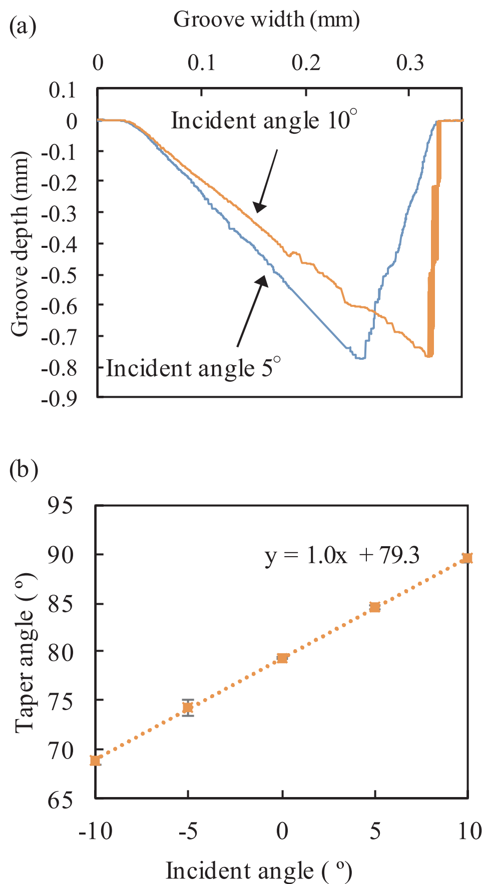

Fig. 22. (a) The cross-sectional profiles of the grooves and (b) their taper angle in relation to the incident angle.

speed resulted in a smaller groove depth at high irradiation times. Furthermore, from Fig. 15b, by applying a higher scanning speed, a lower taper angle was obtained.

This is thought to be due to the smoothing effect which arises when a sufficiently high scanning speed is used. Smoothing only occurred at the higher speed as less pulses are irradiated onto the surface in a given laser pass and machining is carried out in the 'gentle' etch phase (compared to the 'strong' etch phase of the lower speed). In order to investigate this phenomena, the groove bottom was compared and the SEM images are shown in Fig. 16. With a lower scanning speed, a rough surface was observed in Fig. 16a and the increase in surface roughness is presented in Fig. 17. In comparison, with a high scanning speed, regions of high smoothness can be observed in between neighboring passes, as in Fig. 16b and the surface roughness is much lower. The flow of a thin melt layer is known to enable surface smoothing [28]. Additionally, no circular droplets can be observed on the irradiated surface in Fig. 16b as the irradiated energy is insufficient to cause ejection of melted droplets. At a high smoothness, or in other words, at a low surface roughness, the damage threshold increases and it becomes more difficult to machine the surface [25]. Therefore, a smaller depth and taper angle was obtained at a higher scanning speed. This effect becomes more pronounced at later irradiation times as the difference in surface roughness becomes greater.

Furthermore, with regards to the groove machined by a scanning speed of 5 mm/s, the surface may be more difficult to machine with consecutive passes as the transmission rate improves after machining. The transmission rate increases from 50.9% to 67.1% for a wavelength of 532 nm. Thus, less energy is absorbed by the sapphire for machining. Moreover, there are less crystal defects present near the surface. By investigating the X-ray rocking curve as shown in Fig. 18, it was found that the crystallinity improved after laser irradiation; the FWHM (full-width at half maximum) decreased from 23.7 to 19.7, indicating a cleaner single-crystal structure after irradiation. As defects are essential for absorption, heating and material removal to occur, this shows that the machinability of sapphire decreases with consecutive irradiation passes [29,30]. Furthermore, it demonstrates the possibility for laser irradiation to be used as a method to rapidly remove crystal defects. Irradiation, at the correct parameters, can improve surface roughness, transmissivity and crystallinity.

From the SEM images of the groove wall as shown in Fig. 19, micro-cracks are observed in the grooves machined at low speed while small pores are observed at high speed. The cracks may be formed due to laser-induced thermal stress. Due to thermal accumulation, higher maximum temperatures are achieved at lower speeds [31]. This caused greater thermal stress compared to higher scanning speeds. The pores may be formed by limited melting and fluidic movement. This phenomenon was further investigated by measuring the surface roughness. From the results of Fig. 20, the surface roughness of the groove wall was reduced by roughly 1/3 after irradiation. The reduction in surface roughness is due to the flow of the melt layer formed during laser heating. The melt layer experiences surface tension so that the roughness decreases after irradiation [32]. Moreover, it is important to note that the higher speed results in a higher surface roughness. A greater

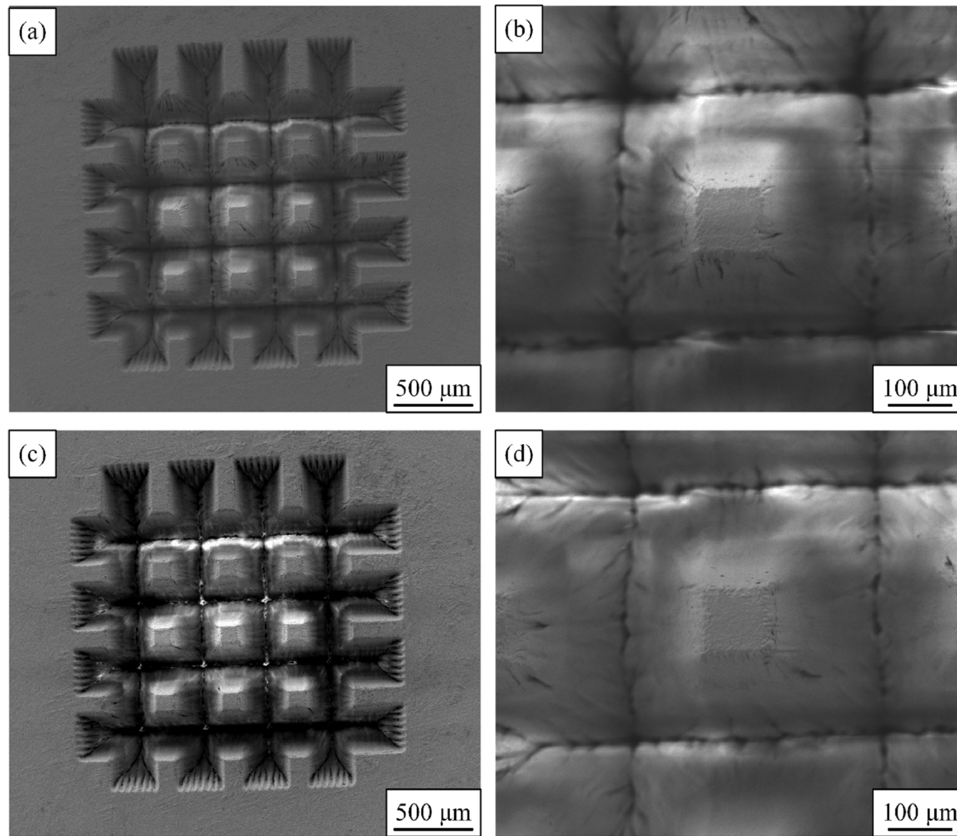

Fig. 23. SEM images of the pyramidal structure machined by (a) 0.5 mm/s and (b) at a larger magnification; (c) 5 mm/s and (d) at a larger magnification.

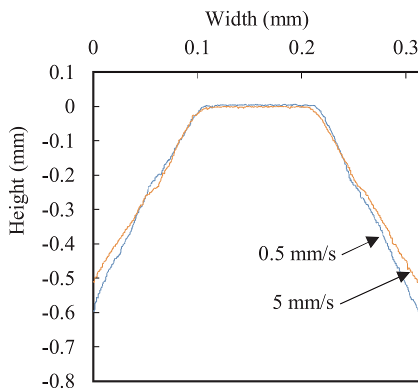

Fig. 24. The cross-sectional profile of a single pyramid.

smoothing effect was observed for the higher speed at the groove bottom; however this trend is reversed at the groove wall. At the groove wall, the fluence is lower than at the groove bottom. Thus with a higher speed, only a partial melt layer is formed. This causes a limited smoothing effect compared to the bottom, resulting in a higher surface roughness when using 5 mm/s and the formation of pores. The pores may be due to the lower melt depth at a higher speed, as energy input into material per pass is lower. This means that there is less fluidic movement so that the pores are not filled. The difference in surface roughness of the groove wall is much smaller than at the groove bottom, thus it is thought to have little effect on the wall machinability.

From the consideration of the current and previous sections, it is possible to divide the mechanism of taper formation into 3 steps, as presented in Fig. 21, divided by number of irradiation times. The first step is the first irradiation where a non-cylindrical mark is machined on a flat surface. This step is driven by the non-uniform Gaussian energy distribution of the laser beam. The energy distribution leads to a temperature distribution and a curved melt front in the irradiated zone. This causes the initial taper to form. In the second step, during the 1st ~5th irradiation, the laser beam is irradiated onto a tilted surface. The focal plane position has no effect throughout the process and the beam is nearly cylindrical. The taper propagates to its maximum value as dictated by the machining threshold. After the taper angle reaches its maximum value, the third step takes place, and the trapezoidal groove develops into a V-shaped groove at a constant taper angle. At these later irradiation times, the scanning speed has a growing effect. With a high scanning speed, a lower surface roughness is obtained at the groove bottom, leading to an increased damage threshold and limited machining.

4.5. Effect of incident angle

In order to establish a method to machine any given taper angle, the effect of the incident angle was investigated. Machining of grooves was carried out at a constant fluence of 15.7 J/cm^2, a scanning speed of 0.5 mm/s and 15 times. The incident angle was changed by tilting the sample. The cross-sectional profiles of the grooves machined by different incident angles, and the resulting taper angles are shown in Fig. 22. The cross-sectional profiles show that a V-shaped groove, that has been rotated an amount equivalent to the incident angle, has been machined.

Fig. 22b shows that the angle of the machined slope is given by the following relation:

$$\theta_{tilt} = \theta_0 + \beta$$

where θ_{tilt} is the angle of the machined slope, θ_0 is the original taper angle and β is the angle at which the laser beam is incident. This indicates that the taper angle θ_0 is not affected by changes in the incident angle β.

By establishing the taper angle machined by irradiation using a

beam perpendicular to the machined surface θ_0, an arbitrary angle θ_{tilt} can be machined by controlling β. In applications where it is necessary, it is possible to machine rectangular grooves in sapphire even with the use of a Gaussian beam. The surface needs to be tilted 11.7° and machined, then tilted −11.7° and machined again. This control over the angle enables the machining of three-dimensional structures using a laser with a simple two dimensional scanning system. On a cautionary note, considering the discussion from the previous section, it would not be possible to machine sapphire when the laser is incident at an angle of greater than 79.3°. The fluence would be too low for machining to occur.

4.6. Machining of pyramidal structures

The pyramidal structures were machined by a laser fluence of 15.7 J/cm^2 and 15 times for a scanning speed of 0.5 mm/s and 150 times for 5 mm/s. The SEM images of the structures are shown in Fig. 23 and the cross-sectional profiles in Fig. 24. From Fig. 23, it is possible to see that 3 × 3 pyramidal structures were successfully machined.

The taper angle is 79.3° and 78.0° for the structures machined by a scanning speed of 0.5 mm/s and 5 mm/s, respectively. This is in agreement with the values obtained by groove machining. Some cracks are visible on the machined surface in Fig. 23b as a lower speed causes greater thermal stress. To prevent microcracks, a higher scanning speed is preferential. The aspect ratios were found to be 2.3 and 2.0 for the surface machined by a scanning speed of 0.5 mm/s and 5 mm/s, respectively. Such structures are known to have a reflectivity of < 3% within the frequency range of 170–300 GHz [17], which is usable in the given application for CMB measurement. Some improvements need to be made in the future to achieve a greater aspect ratio and thus a wider low-reflectivity range.

5. Conclusions

The mechanism behind taper formation during the laser irradiation of deep V grooves on single-crystal sapphire was investigated. It was found that:

1. A taper develops at a low number of irradiation times and this angle is maintained throughout the development of the groove. Laser fluence and the ablation threshold of the material determine the taper angle. As the taper angle increases, the incident fluence decreases; once the incident fluence reaches the ablation threshold, no more machining can take place and the taper angle becomes constant. However, when the Rayleigh length is large, focal plane position does not affect the taper angle.
2. Scanning speed affects the taper angle due to a smoothing effect. A greater smoothing effect was observed for the higher speed at the groove bottom; this decreased the machinability of the surface. However, this smoothing trend was reversed at the groove wall.
3. A given groove shape can be machined by controlling the incident angle of the laser and considering the taper angle.
4. A 3-dimensional micro-pyramid structure can be machined, by using only a 2-dimensional laser scanning system.

By applying the taper formation mechanism in laser micromachining, the machining of sharp microstructures with steep walls was possible. Further investigations will be carried out to improve the surface quality and aspect ratio of the micro-pyramid structure. In addition, attempts will be made to investigate the taper formation mechanism on other ceramic materials.

References

[1] Shamir A, Ishaaya AA. Applied Surface Science Large volume ablation of Sapphire with ultra-short laser pulses. Appl Surf Sci 2013;270:763–6.
[2] Lee JH, Hwang SM, Kim NS, Lee JH. InGaN-based high-power flip-chip LEDs with deep-hole-patterned sapphire substrate by laser direct beam drilling. IEEE Electron Device Lett 2010;31:698–700.
[3] Chang CW, Chen CY, Chang TL, Ting CJ, Wang CP, Chou CP. Sapphire surface patterning using femtosecond laser micromachining. Appl Phys a-Materials Sci Process 2012;109:441–8.
[4] Katahira K, Matsumoto Y, Komotori J, Yamazaki K. Experimental investigation of machinability and surface quality of sapphire machined with polycrystalline diamond micro-milling tool. Int J Adv Manuf Technol 2017;93:4389–98.
[5] T.R. Anthony, R.J. Connery, D.F. Hoeschele, United States Patent 4, 437, 1984,109.
[6] Jia H, Guo L, Wang W, Chen H. Recent progress in GaN-based light-emitting diodes. Adv Mater 2009;21:4641–6.
[7] S. Huang, R. Horng, K. Wen, Y. Lin, K. Yen, D. Wuu, Improved light extraction of nitride-based flip-chip light-emitting diodes via sapphire shaping and texturing, 18 2006, 2623–2625.
[8] Ashkenasi D, Müller G, Rosenfeld A, Stoian R, Hertel IV, Bulgakova NM, et al. Fundamentals and advantages of ultrafast micro-structuring of transparent materials. Appl Phys A Mater Sci Process 2003;77:223–8.
[9] Kuar AS, Doloi B, Bhattacharyya B. Modeling and analysis of pulsed Nd:YAG laser machining characteristics during micro-drilling of zirconia(ZrO2). Int J Mach Tools Manuf 2006;46:1301–10.
[10] Li L, Low DKY, Ghoreshi M, Crookall JR. Hole taper characterisation and control in laser percussion drilling. CIRP Ann − Manuf Technol 2002;51:153–6.
[11] Yilbas BS. Investigation into drilling speed during laser drilling of metals. Opt. Laser Tech. 1988;20:29–32.
[12] Ghoreishi M, Low DKY, Li L. Comparative statistical analysis of hole taper and circularity in laser percussion drilling. Int J Mach Tools Manuf 2002;42:985–95.
[13] Yang L, Ding Y, Cheng B, Mohammed A, Wang Y. Numerical simulation and experimental research on reduction of taper and HAZ during laser drilling using moving focal point. Int J Adv Manuf Technol 2016:1–10.
[14] Bhuyan MK, Courvoisier F, Lacourt PA, Jacquot M, Furfaro L, Withford MJ, et al. Ultrafast Bessel beams for high aspect ratio taper free micromachining of glass. Proc of SPIE 2010;7728. 77281 V.
[15] Shen H, Feng D, Yao Z. Modeling of underwater laser drilling of alumina. J Manuf Sci Eng 2017;139:1–10.
[16] Southwell WH. Pyramid-array surface-relief structures producing antireflection index matching on optical surfaces. J Opt Soc Am A 1991;8:549–53.
[17] Schütz V. Laser processing of sub-wavelength structures on sapphire and alumina for millimeter wavelength broadband anti-reflection coatings. J Laser Micro/Nanoeng 2016;11:204–9.
[18] Ruettimann C, Dury N, Woratz C, Woessner S. Sapphire cutting with pulsed fiber lasers. Proc ICALEO 2013:720–4.
[19] Harilal SS, Bindhu CV, Tillack MS, Najmabadi F, Gaeris AC. Internal structure and expansion dynamics of laser ablation plumes into ambient gases. J Appl Phys 2003;93:2380–8.
[20] Barthélemy O, Margot J, Chaker M, Sabsabi M, Vidal F, Johnston TW, et al. Influence of the laser parameters on the space and time characteristics of an aluminum laser-induced plasma. Spectrochim Acta − B At Spectrosc 2005;60:905–14.
[21] Körner C, Mayerhofer R, Hartmann M, Bergmann HW. Physical and material aspects in using visible laser pulses of nanosecond duration for ablation. Appl Phys A 1996;63:123–31.
[22] Zhu S, Lu YF, Hong MH, Chen XY. Laser ablation of solid substrates in water and ambient air. J Appl Phys 2001;89:2400–3.
[23] Trtica MS, Gakovic BM, Radak BB, Batani D, Desai T, Bussoli M. Periodic surface structures on crystalline silicon created by 532 nm picosecond Nd:YAG laser pulses. Appl Surf Sci 2007;254:1377–81.
[24] Wu Q, Ma Y, Fang R, Liao Y, Yu Q, Chen X, et al. Femtosecond laser-induced periodic surface structure on diamond film. Appl Phys Lett 2003;82:1703–5.
[25] Lowdermilk WH, Milam D. Laser-induced surface and coating damage. IEEE J Quant Electron 1981;17:1888–903.
[26] Brailovsky AB, Gaponov SV, Luchin VI. Mechanisms of melt droplets and solid-particle ejection from a target surface by pulsed laser action. Appl Phys A Mater Sci Process 1995;61:81–6.
[27] Kamalu J, Byrd JP. Statistical design of laser drilling experiments. Proc ICALEO Sect B 1998;98:264–73.
[28] Mendez E, Nowak KM, Baker HJ, Villarreal FJ, Hall DR. Localized CO2 laser damage repair of fused silica optics. Appl Opt 2006;45:5358–67.
[29] Feit MD, Rubenchik AM. Influence of subsurface cracks on laser induced surface damage. Proc SPIE 2004;5273:264–72.
[30] Bloembergen N. Role of cracks, pores, and absorbing inclusions on laser induced damage threshold at surfaces of transparent dielectrics. Appl Opt 1973;12:661–4.
[31] Attar H, Calin M, Zhang LC, Scudino S, Eckert J. Manufacture by selective laser melting and mechanical behavior of commercially pure titanium. Mater Sci Eng A 2014;593:170–7.
[32] Hrma P, Han WT, Cooper AR. Thermal healing of cracks in glass. J Non Cryst Solids 1988;102:88–94.